EEET ECOLOGICAL ENGINEERING & ENVIRONMENTAL TECHNOLOGY

Ecological Engineering & Environmental Technology, 2026, 27(9), 223–239
https://doi.org/10.12912/27197050/226295
ISSN 2719–7050, License CC-BY 4.0

Received: 2026.07.05
Accepted: 2026.08.03
Published: 2026.08.15

Time-domain analysis of reactive power compensation for voltage stability in wind-integrated power networks

Kadhim Hamzah Chalok[1*], Karrar Hameed Kadhim[2]

[1] Center for Research on Environment and Renewable Energy, University of Kerbala, 56001 Karbala, Iraq
[2] AL-Musaib Technical College, Al-Furat Al-Awsat Technical University, 51002 Babylon, Iraq
* Corresponding author's e-mail: kadhim.hamzah@uokerbala.edu.iq

ABSTRACT

This paper presents a time-domain simulation study of dynamic reactive power compensation for voltage stability in a wind-integrated power system. A 50 MW doubly-fed induction generator (DFIG) wind farm is connected at bus 9 of the IEEE 14-bus network, comparing two technologies: a Static Synchronous Compensator (STATCOM) with a PI voltage regulator and anti-windup, and a static VAR compensator (SVC) with a thyristor-controlled reactor and first-order lag dynamics. Bus voltages are computed via a full Newton-Raphson power-flow solver on the complete 14 × 14 admittance matrix. Wind speed is modelled using an AR (1) process calibrated to IEC 61400 Class B conditions. Simulations span seven mean wind speeds (3–18 m/s) at 30% penetration, plus a sensitivity analysis across five penetration levels (10–50%) at rated speed. STATCOM reduces bus-9 voltage deviation from 2.79–2.97% to 0.61–0.80% (73–79% reduction); SVC achieves only 59–65% reduction with larger residual fluctuations. This advantage is confirmed by a Monte Carlo analysis (N = 15 independent AR(1) realisations per operating point), which shows STATCOM outperforming SVC at every tested wind speed with high statistical significance ($p < 0.001$, Wilcoxon signed-rank test), and reproduces on an independent, larger IEEE 30-bus network. Both compensators slightly increase network-wide reactive losses relative to the uncompensated case on the IEEE 14-bus network (STATCOM: +2.9 to +4.4%; SVC: +2.5 to +3.5%). Within the investigated simulation scenarios, both compensators maintained stable operation across all tested wind penetration levels (10–50%) on both networks.

Keywords: wind energy integration, voltage stability, reactive power compensation, STATCOM, static VAR compensator, doubly-fed induction generator, Newton–Raphson power flow.

INTRODUCTION

The accelerating global deployment of wind energy – driven by carbon neutrality targets and declining turbine costs – has transformed the composition of power systems worldwide. In 2023, global installed wind capacity surpassed 1.000 GW, as installations onshore and offshore expanded rapidly into networks that were originally designed around centralised synchronous generation [1, 2]. This fundamental change brings unique challenges for voltage stability of the power system: wind turbines based on DFIGs do not inherently provide the reactive power support provided by conventional synchronous machines and, in addition, their stochastic output – driven by the variability of wind speed – generates continuous reactive power imbalances at the point of connection that, without adequate control, can result in voltage collapse or persistent deviation from statutory limits [3, 4]. Reactive power compensation and voltage stability for wind-integrated networks have been the focus of a large body of work, organised into three broad strands: (i) STATCOM-focused studies, (ii) SVC- and FACTS-oriented research works, and (iii) the modelling frameworks employed to assess these devices. On the STATCOM side, Sharma et al. [5] provide a comprehensive bibliographic review covering STATCOM modelling, control, stability, optimal location, integration, and field installations, compiled over 16 years of research, concluding that dynamic reactive power support and optimal siting remain active research fronts despite the technology's maturity. Focusing specifically on wind integration, Yang and Chang [6] proposed a multi-objective optimisation strategy for STATCOM capacity and location under seasonal wind power variability, showing that reactive power compensation requirements are sensitive to the statistical distribution of wind output rather than to a single design wind speed a finding that motivates the multi-operating-point approach adopted in the present study. Al-Majali and Zobaa [7] further formulated STATCOM sizing and siting as a joint cost/voltage-deviation optimisation problem, confirming that the economic and technical benefits of STATCOM compensation are highly location-dependent.

On the SVC and FACTS side, Adetokun and Muriithi [8] reviewed the application and control of FACTS devices for voltage stability enhancement in renewable-integrated grids, and Alajrash et al. [9] more recently surveyed SVC, STATCOM, TCSC, UPFC and distributed power-flow-controller technologies for power quality and stability under renewable penetration. Both reviews conclude that SVC's thyristor-based susceptance control is inherently slower and more prone to residual oscillation than converter-based STATCOM. Complementing these device-level reviews, Gao et al. [10] specifically reviewed dynamic voltage support technologies and aggregation modelling for power grids with large-scale wind and PV penetration, while Khan et al. [11] reviewed grid-forming converter control for inverter-based resources more broadly, noting that STATCOM-class converters are increasingly expected to provide grid-forming as well as grid-following support as penetration increases. A smaller set of studies directly compares STATCOM and SVC performance for DFIG-based wind farms. Mahmoud et al. [12] evaluated SVC and STATCOM alongside a fixed capacitor bank for fault-ride-through capability and voltage stability under various wind speed and fault events, finding that STATCOM provides faster voltage recovery at lower reactive capacity, while Sadiq et al. [13] reviewed STATCOM control strategies for wind/PV-penetrated systems and identified coordinated control between the compensator and wind-farm reactive capability as an open research direction. Chirani et al. [14] tuned an SVC's PI voltage controller for a grid-connected DFIG wind farm using metaheuristic optimisation and confirmed that SVC performance is highly sensitive to controller gain scheduling under wind speed variability. Complementary work by Tariq et al. [15] compared reactive power compensation devices in a real electrical substation, and Rehman et al. [16] examined optimal reactive power compensation for HVAC-connected offshore wind farms; both conclude that compensation-technology selection has a first-order effect on network losses and voltage-limit compliance. Sakipour and Abdi [17] proposed a self-correcting SVC coordinated with battery energy storage to damp wind-farm voltage and reactive power oscillations, illustrating a hybridisation direction. On the STATCOM side specifically for DFIG wind farms, Muisyo et al. [18] tuned a STATCOM controller with metaheuristic algorithms to enhance low-voltage ride-through of a DFIG wind power plant, and Borah et al. [19] proposed a reinforcement-learning-based coordinated transient controller for real-time reactive power sharing between a DFIG wind farm and a STATCOM, validated – as in the present study – on the IEEE 14-bus test system; however, their work optimises rotor-angle and grid-code compliance metrics through a learned control policy rather than providing a systematic, PI/TCR-governed head-to-head dynamic comparison of STATCOM against SVC across a full wind-speed and penetration sweep.

Despite this substantial literature, the majority of these studies evaluate compensator performance using a single-bus or point-of-common-coupling equivalent, in which a fixed Thevenin source or a simplified two-bus feeder represents the remainder of the network. Hiwarkar et al. [20] demonstrate the standard full Newton-Raphson load-flow formulation for the IEEE 14-bus network, but do not incorporate a wind farm or dynamic FACTS control. Consequently, the interaction between a wind-farm compensator and the voltage response at electrically adjacent load buses show to be significant – has not been characterised for STATCOM and SVC side-by-side on a full multi-bus benchmark network. This is the principal gap addressed by the present study. Beyond the FACTS-specific literature, several broader studies inform the present work. Hoke et al. [21] examined the stability and reliability challenges of island power systems with high levels of inverter-based resources, underscoring the growing importance of fast, converter-based reactive support, such as the STATCOM modelled here. Ranjan and Shankar [22] surveyed load-frequency control strategies amid increasing renewable energy integration, highlighting that active- and reactive-power control problems are increasingly coupled as penetration rises. Finally, the present authors' own earlier work demonstrated effective PI and LQR control for DFIG pitch regulation [23], providing the control-design foundation that the STATCOM and SVC voltage-loop builds upon.

This paper addresses this gap by implementing a full time-domain simulation framework on the IEEE 14-bus benchmark network, with the complete 14 × 14 admittance matrix and Newton-Raphson power flow solved at each simulation time step. The present work advances beyond prior contributions in this area, including the authors' own earlier work on DFIG pitch control, and the broader literature on inverter-based resource stability, load frequency control under renewable integration, and voltage stability at high renewable penetration. The main contributions of this work are summarised as follows:

1. A full multi-bus time-domain simulation framework providing a head-to-head dynamic comparison of PI-governed STATCOM and TCR-based SVC on the IEEE 14-bus benchmark network;
2. An IEC 61400-calibrated AR(1) turbulence model for realistic wind-speed variability;
3. A penetration sensitivity analysis spanning 10–50% wind penetration at rated wind speed;
4. A Monte Carlo statistical validation of the STATCOM-SVC comparison across N = 15 independent wind-turbulence realisations; and
5. A generalisation check on an independent, larger IEEE 30-bus network.

BACKGROUND

Voltage stability, as formally defined and classified by the IEEE/CIGRE joint task force [24], is the ability of a power system to maintain steady, acceptable voltages at all buses following a disturbance. FACTS devices such as STATCOM and SVC are widely used to provide dynamic reactive power support at points of common coupling where renewable generation is connected [15]. For a lossless transmission line connecting buses i and j, the reactive power delivered to bus j is

$$Q = \mathrm{VIsin}\,\phi \tag{1}$$

where: V is the voltage magnitude (kV), I is the line current (A), and ϕ denotes the voltage–current phase angle.

The active power transfer is given by:

$$P = \frac{V_1 V_2}{X} \sin\delta \tag{2}$$

where: X is the transmission line reactance (Ω) and δ is the power angle between the sending-end and receiving-end voltages.

The active power output of the wind turbine is represented by the standard cubic power curve:

$$P_w = P_r \left(\frac{v - v_{ci}}{v_r - v_{ci}}\right)^3, \tag{3}$$
$$P_w = 0, v < v_{ci}, P_w = P_r, v_r \le v \le v_{co}$$

where: P_r is the rated wind-farm capacity (MW), which scales with the tested wind penetration level (Pr = penetration fraction × 100 MVA; e.g. 30 MW at 30% penetration), v_{ci} = 3 m/s is the cut-in wind speed, and v_r = 12 m/s is the rated wind speed.

The reactive power absorbed by the DFIG-based wind farm from the grid is modelled as:

$$Q_w(P_w) = Q_t + k_q P_w, Q_t = \tag{4}$$
$$= 4.0\, MVAr, k_q = 0.28$$

where: Q_t is the constant transformer magnetising reactive power demand, and $k_q P_w$ represents the stator reactive power demand, which is assumed to be proportional to the active power output.

The voltage drop along the equivalent feeder is expressed as:

$$\Delta V = IZ \tag{5}$$

The Newton-Raphson power flow update at each iteration is:

$$J \begin{bmatrix} \Delta\theta \\ \frac{\Delta V}{V} \end{bmatrix} = \begin{bmatrix} \Delta P \\ \Delta Q \end{bmatrix} \tag{6}$$

where: J is the full $2(n-1) \times 2(n-1)$ Newton–Raphson Jacobian matrix, which is updated at each iteration using the current bus voltage magnitudes and voltage angle estimates for all $n = 14$ buses.

The voltage correction vector consists of the bus voltage angle increments ($\Delta\theta$) and the normalized voltage magnitude increments ($\Delta V / V$), while the mismatch vector comprises the active and reactive power mismatches (ΔP, ΔQ). The STATCOM PI control law with anti-windup is expressed as:

$$Q_{comp}(t) = K_p e_V + K_i \int e_V dt, \quad K_p = 2.0,\ K_i = 0.6 \tag{7}$$

where: K_p is the voltage error expressed in per unit (p.u.), and K_p is limited to the operating range of MVAr to represent the reactive power capability of the STATCOM.

An anti-windup back-calculation mechanism is incorporated to prevent integrator saturation during large voltage deviations. This single-loop PI structure with anti-windup back-calculation follows established PI design practice for AVR and FACTS voltage controllers, consistent with the tuning principles discussed by Micev et al. [25]. The SVC thyristor-controlled reactor (TCR) is represented by a first-order dynamic model, consistent with the coordinated SVC/STATCOM control strategies reviewed by Sadiq et al. [13] and subsequently applied to DFIG-based wind farms by Chirani et al. [14], as follows:

$$e_v(t) = V_{ref} - V_{meas}(t) Q_{comp} \pm 20$$
$$T_{svc} \frac{dQ_{svc}}{dt} = = Q_{ref} - Q_{svc}, T_{svc} = 0.05\ s \tag{8}$$

where: $Q_{ref} = K_{p,svc} e_v$ is the proportional reactive power reference, with $K_{p,svc} = 15$, and $e_v = V_{ref} - V_{meas}$ is the voltage error in per unit.

The reactive power ramp rate is limited to ±10 MVAr/s to represent the practical switching response of the thyristor-controlled reactor (TCR), and the SVC output magnitude is additionally clipped to the same ±20 MVAr operating range as the STATCOM (Equation 7). The voltage stability index (VSI) at Bus 9 is defined as:

$$VSI = \frac{V_9}{V_{slack}} \tag{9}$$

where: V_9 and V_{slack} are the voltage magnitudes at Bus 9 and the slack bus, respectively.

Values of *VSI* below 0.95 are considered indicative of unacceptable voltage performance. The system-wide reactive power losses are computed as:

$$Q_{loss} = \sum_{k=1}^{m} I_k^2 X_k \quad (\textit{summed over all } 20 \textit{ branches}) \tag{10}$$

where: I_k is the current flowing through branch, k, X_k is the branch reactance, and $m = 20$ is the total number of transmission branches in the IEEE 14-bus system.

The total reactive power loss is obtained by summing the reactive losses over all transmission branches.

$$v(k) = \bar{v} + \alpha[v(k-1) - \bar{v}] + \varepsilon(k), \quad \varepsilon(k) \sim \mathcal{N}, \left(0, \sigma^2(1-\alpha^2)\right) \tag{11}$$

where: $\bar{v}$ is the mean wind speed, $\alpha = \exp(-\Delta t/\tau)$ is the autocorrelation coefficient, $\tau = 15$ s is the turbulence time constant, and $\sigma = \text{TI}\ \bar{v}$, where TI = 0.08 corresponds to the turbulence intensity specified for IEC 61400 Class B wind conditions.

The first-order autoregressive (AR(1)) model captures the short-term temporal correlation of wind speed fluctuations, providing a more realistic representation of wind variability than static probability distribution models, such as the Weibull-based approaches compared by Teimourian *et al.* [26].

Test network and simulation framework

The IEEE 14-bus benchmark network is used as the test system: two synchronous generators (buses 1 and 2), three synchronous condensers (buses 3, 6, and 8), 20 transmission branches, and 9 load buses. A 50 MW DFIG wind farm is connected at bus 9, a moderately loaded bus (P9 = 29.5 MW, Q9 = 16.6 MVAr) with high reactive power sensitivity due to its distance from generation buses. The full 14 × 14 admittance matrix Y-bus is constructed from the published IEEE 14-bus branch data, following the load-flow formulation validated on this network by Hiwarkar et al. [20], and is used without reduction or approximation. The complete simulation framework—Y-bus construction, the Newton-Raphson power-flow solver, the DFIG/wind model, and the STATCOM/SVC dynamic controllers – was implemented in Python, using NumPy for matrix and linear-algebra operations, with all differential equations (Equations 7, 8, 11) integrated via explicit fixed-step time stepping at Δt = 0.5 s. Figure 1 illustrates the power system architecture including wind farm integration and FACTS device placement.

Newton-Raphson power flow

At each simulation time step (Δt = 0.5 s), bus voltages at all 14 buses are updated by running a Newton-Raphson power flow on the full Y-bus matrix with the current DFIG active and reactive power injections and STATCOM/SVC reactive output. The N-R solver uses up to 8 iterations with a convergence tolerance of 10^{-5} p.u. on the power mismatch vector. PV bus voltages (buses 2, 3, 6, 8) and the slack bus voltage (bus 1) are held constant per iteration; PQ bus voltages (buses 4, 5, 7, 9–14) are updated using the full Jacobian. This approach correctly captures the interaction between the compensator reactive power injection at bus 9 and the voltage response at all adjacent buses (10, 11, 14), which single-bus equivalent models cannot represent. The same Newton–Raphson solution procedure, reimplemented for the 30-bus admittance matrix, was applied to the IEEE 30-bus benchmark network for the independent generalisation check.

Wind farm and DFIG model

The DFIG wind farm is modelled as a lumped equivalent unit with rated capacity Pr = penetration × Sbase (MW), i.e., 30 MW at 30% penetration. Active power follows the cubic power curve (Equation 3). Reactive power demand follows the calibrated DFIG model of Equation 4, where the 4 MVAr transformer magnetising demand is present whenever the turbine is connected (v ≥ 3 m/s), and the stator term 0.28·Pw increases linearly with active output. At rated wind speed (v = 12 m/s, Pw = 30 MW), the total reactive demand is Qw = 4 + 0.28 × 30 = 12.4 MVAr. Wind speed time series are generated by the AR(1) model (Equation 11) with T = 600 s, Δt = 0.5 s, giving 1.200 time steps per scenario. For the statistical validation, 15 independent AR(1) wind-speed realisations were generated for each operating point

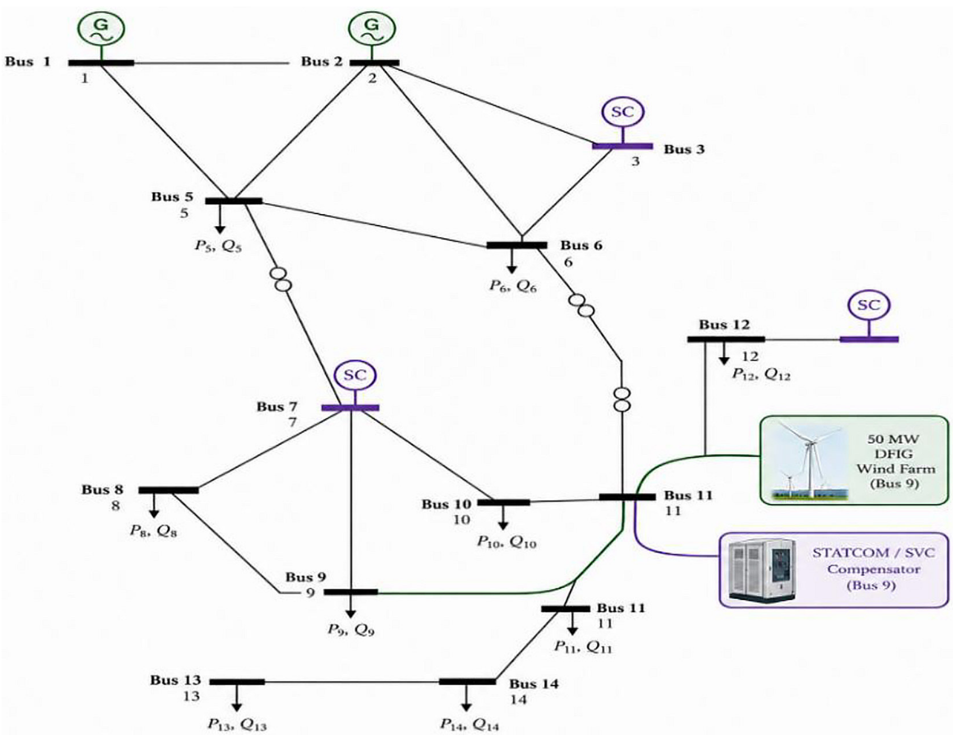

Figure 1. IEEE 14-bus power system architecture with DFIG wind farm at bus 9 and STATCOM/SVC compensation

by varying only the random seed while holding all other AR(1) parameters (τ, TI, and hence α and σ) fixed; the resulting 15 datasets per operating point were used as the Monte Carlo sample. Figure 2 illustrates the key mechanical and electrical components of the DFIG wind turbine, consistent with the DFIG converter and generator structure described by Desalegn et al. [27].

STATCOM and SVC models

The STATCOM is modelled as a voltage-source converter with continuous reactive power output governed by the PI controller of Equation 7, evaluated at each 0.5 s simulation time step against the Bus 9 voltage returned by the Newton-Raphson power flow. Anti-windup is implemented by back-calculating the integral state whenever the output saturates at the ±20 MVAr rating. The SVC TCR is modelled by Equation 8 with a first-order lag (T_{svc} = 0.05 s) and proportional control (Kp_{svc} = 15), consistent with the self-correcting SVC control philosophy proposed by Sakipour and Abdi [17] (the present study models the SVC alone, without the battery energy storage coordination examined in that work) and with the PI-tuned SVC applied to a grid-connected DFIG wind farm by Chirani et al. [14], and is broadly consistent with the wind-farm voltage control taxonomy (QV control and voltage droop control) reviewed by Wu et al. [28]. Rate limiting (±10 MVAr/s) reflects the physical constraint that thyristor firing angle cannot change instantaneously. This results in the SVC having a noticeably slower response to turbulence-driven voltage transients than the STATCOM, as captured in the dynamic simulation results. The STATCOM and SVC parameter values used throughout this study – Kp = 2.0 and Ki = 0.6 for the STATCOM, Kp, svc = 15 and Tsvc = 0.05 s for the SVC, and the ±20 MVAr output limit for both – are held fixed across every wind speed, every penetration level, all 15 Monte Carlo replications and the independent IEEE 30-bus network.

No controller retuning is performed for any scenario or network, so that the reported STATCOM-SVC comparisons isolate the effect of the operating condition and network topology rather than any difference in controller tuning. Figure 3 illustrates the general wind turbine subsystem architecture and the placement of the STATCOM/SVC voltage control loop at the point of common coupling, in the style of the turbine subsystem diagrams used by Shawqran et al. [29]; blade-pitch actuation itself is not dynamically modelled in the present study, which represents wind-turbine active power output through the algebraic power curve of Equation 3.

Simulation scenarios

Two sets of scenarios are run. The main scenarios cover seven mean wind speeds (3, 5, 7, 9, 12, 15, 18 m/s) at 30% penetration for three compensation configurations: no compensation (System 1), STATCOM (System 2), and SVC (System 3). The sensitivity analysis covers five penetration levels (10, 20, 30, 40, 50%) at v = 12 m/s for all three configurations. KPIs computed from each 600-second simulation are: RMS voltage deviation Vd (%), system reliability rel (% time

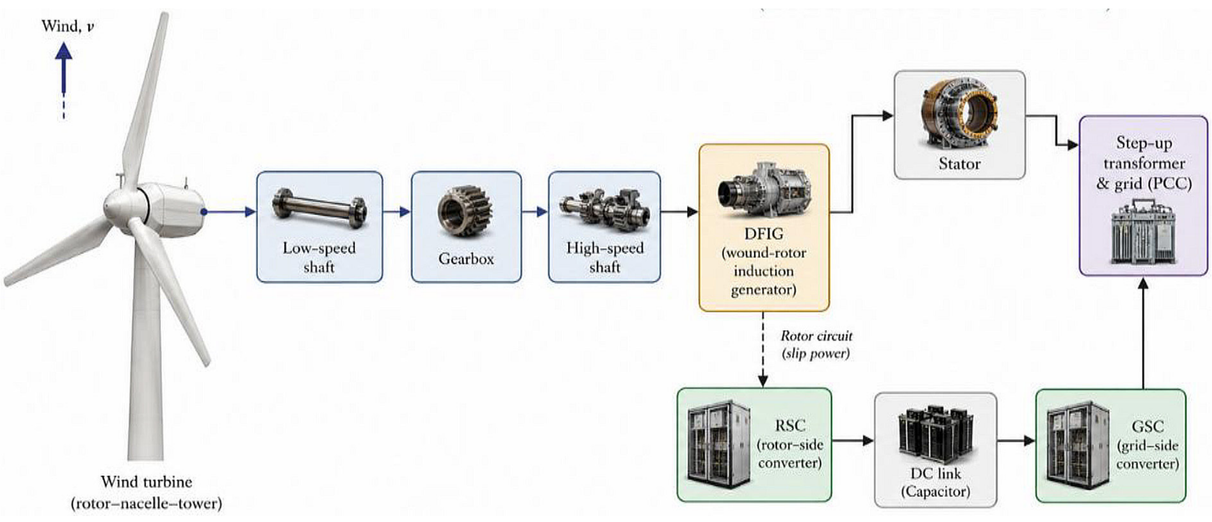

Figure 2. DFIG wind turbine with key components

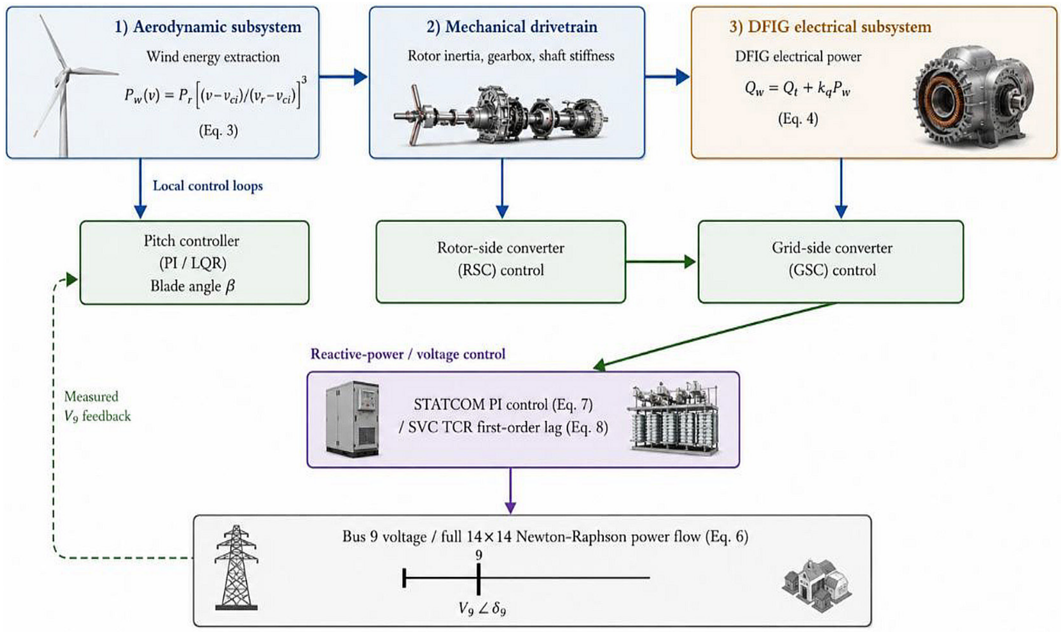

Figure 3. Wind turbine subsystem diagram showing DFIG mechanical–electrical coupling and the STATCOM/SVC control loop

V9 [0.95, 1.05] p.u.), mean reactive power losses Qloss (MVAr, summed over all 20 branches), VSI = V9/V_slack, and mean compensator reactive output Qc (MVAr). To evaluate the statistical robustness of the STATCOM-SVC comparison, a Monte Carlo analysis was additionally performed for the main wind-speed sweep using N = 15 independent AR(1) wind-speed realisations per operating point; the statistical significance of the STATCOM-SVC difference at each wind speed was assessed using a two-sided Wilcoxon signed-rank test at a significance level of α = 0.05. The same simulation framework, with the identical controller settings described in Section "STATCOM and SVC Models", was independently applied to the IEEE 30-bus benchmark network to examine the generalisability of the STATCOM-SVC comparison beyond the IEEE 14-bus network.

Data, code, and reproducibility statement

To enhance the reproducibility of this study, the complete Python implementation of the proposed simulation framework – including the Y-bus construction, the Newton–Raphson power-flow solver, the DFIG active and reactive power model, the AR(1) wind-speed generator, the Monte Carlo and Wilcoxon statistical-analysis routines, and the dynamic STATCOM and SVC control algorithms – is available from the corresponding author upon reasonable request. The branch and bus data used to form the network admittance (Y-bus) matrix associated with the standard IEEE 14-bus benchmark system [20] are included in Appendix A, while all simulation parameters, including those of the DFIG model, AR(1) wind model, STATCOM, and SVC controllers, as well as a Newton–Raphson solver, are consolidated in Appendix B. These materials provide a transparent and comprehensive description of the proposed methodology and allow for independent reproduction of reported simulation results.

RESULTS AND DISCUSSION

Voltage deviation and system reliability

The RMS voltage deviations and the system reliability indices for the three different investigated configurations are illustrated in Figure 4 over the seven wind-speed operating points. The uncompensated system (System 1, orange) has a mean voltage above 1.0 p.u., whereas the IEEE 14-bus benchmark has a base-case voltage of 1.034 p.u. at bus 9. However, wind-speed turbulence induces RMS voltage fluctuations of 2.79–2.97%. The steady root mean square (RMS) voltage deviation is reduced to 0.61–0.80% (73–79% reduction) by the STATCOM (System 2, blue) through continuous dynamic reactive power support. the SVC (System 3, green) performs moderately well with a nominal total RMS voltage deviation of 1.01–1.16% (59–65% reduction), but its first-order dynamic response limits its ability to compensate for rapid voltage fluctuations. As shown in Fig. 4(b), under the investigated operating conditions, all three configurations provide a 100% reliability index. This result is mainly due to the high pre-disturbance voltage at bus 9 (1.034 p.u.) and the moderate reactive power demand of the 50 MW DFIG wind farm, which prevents the bus voltage from falling below the adopted 0.95 p.u. threshold. Consequently, the reliability index does not provide sensitive distinctions of the dynamic performance of compensation strategies in this benchmark system. On the other hand, the RMS voltage deviation may serve as a more informative measure of controller performance and clearly highlights the superior voltage regulation capability of the STATCOM compared with an SVC. This observation is further investigated statistically using Monte Carlo simulations on identically distributed independent AR(1) wind-speed realisations.

Table 1 provides further insight into the wind-speed dependence of voltage regulation performance that is not readily apparent from Figure 4 alone. Two distinct patterns can be identified. First, Vd_1 and Vd_2 both decrease monotonically with increasing wind speed, from 2.97% to 2.79% and from 0.80% to 0.61%, respectively. Vd_3 (SVC), in contrast, exhibits a non-monotonic response: it decreases to 1.04% at v = 9 m/s, increases to a local maximum of 1.16% at v = 12 m/s (rated wind speed), and subsequently declines to 1.01–1.02% at higher wind speeds This non-monotonic behaviour suggests that the SVC's proportional controller is more sensitive to the network operating point at rated wind speed, where the DFIG's active-power injection reaches its maximum. Second, the Qc_STATCOM column changes by only 0.05 MVAr (19.77 to 19.72) across the full 3-18 m/s range, a variation of about 0.25%; the STATCOM's mean reactive output is therefore set almost entirely by the fixed voltage-error target rather than by wind speed itself, consistent with a well-tuned PI controller operating well within its 20 MVAr limit. This behaviour is consistent with the expected response of a well-tuned PI-controlled

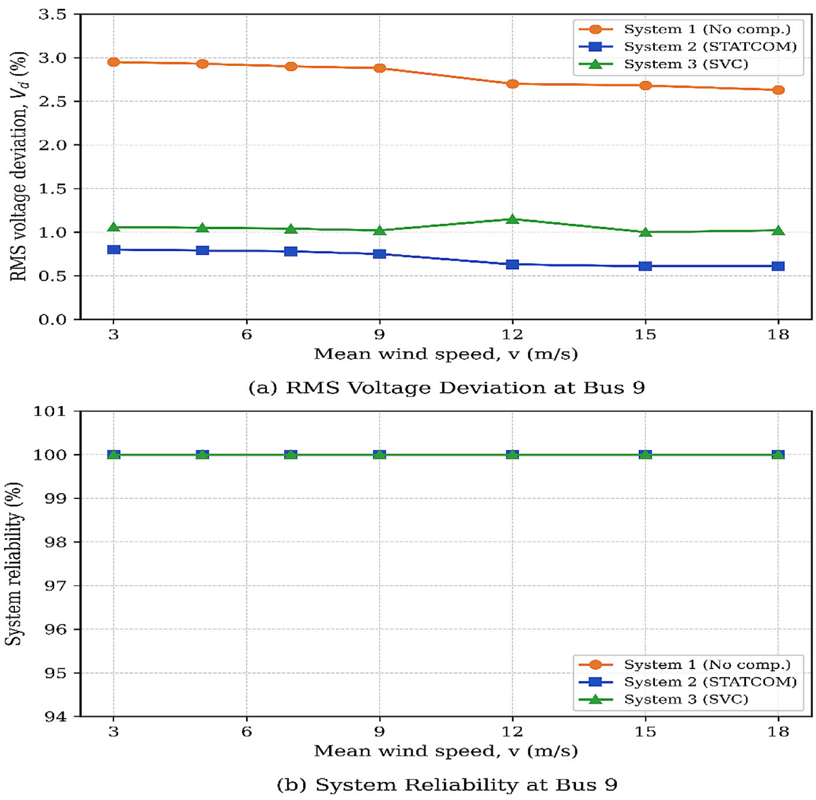

Figure 4. RMS voltage deviation (a) and system reliability (b) for Systems 1, 2, and 3 across wind speeds. IEEE 14-bus N-R, 30% penetration

STATCOM operating within its reactive power limits, and with its consistently lower RMS voltage deviation relative to the SVC's slower, thyristor-based first-order response.

STATCOM and SVC dynamic response comparison

Figure 5 presents the dynamic bus 9 V (Figure 5a) and compensator reactive power output (Figure 5b) for the first 120 s of simulation, with v = 9 m/s shown in the left column and v = 18 m/s in the right column. The first 120 s are presented for clarity, as the remaining simulation exhibits the same qualitative dynamic behaviour. The time-domain traces reveal clear differences in transient behaviour between the two compensators. At v = 9 m/s, the uncompensated voltage (orange) fluctuates around 1.029 p.u. due to turbulence-driven oscillations, whereas the STATCOM (blue) rapidly settles to 1.008 p.u., exhibiting a 10-second PI transient response from startup; the SVC (green) follows a similar trajectory but displays higher-frequency residual oscillations, attributable to its 0.05 s first-order lag and rate limiter. This difference becomes more pronounced at v = 18 m/s: the STATCOM settles stably at approximately 1.006 p.u. within 15 seconds and remains essentially constant thereafter, whereas the SVC exhibits persistent oscillations of ±0.008 p.u., arising from the interaction between its proportional control, rate limiter, and the 0.5 s discrete-time update. These dynamic characteristics are consistent with the lower RMS voltage deviations reported in Table 1 and further support the superior transient voltage regulation provided by the STATCOM. In the compensator-output panels, the STATCOM's reactive power output ramps down smoothly and stabilises at approximately 19.7 MVAr, whereas the SVC output exhibits substantially higher variability. To verify that this advantage does not depend on a single stochastic wind realisation, through a Monte Carlo analysis involving multiple independent AR(1) wind-speed realisations.

VSI and system-wide reactive losses

Figure 6 presents the voltage stability index (Figure 6a) and system-wide reactive power losses summed over all 20 IEEE 14-bus branches (Figure 6b). The VSI ranges from 0.969–0.971 (System 1) to 0.949–0.951 (System 2) across wind speeds, both above the 0.95 threshold. System 3 (SVC) achieves VSI = 0.952–0.954. The slight reduction in VSI with STATCOM compensation can be attributed to the reactive power exchange between the STATCOM and the network, which regulates the bus voltage toward its reference value while slightly increasing feeder reactive current.

Reactive losses (Figure 6b) range from approximately 49.7–66.8 MVAr system-wide across wind speeds and compensation types. STATCOM and SVC compensation both slightly increase system-wide reactive losses relative to the uncompensated case (STATCOM: +2.9 to +4.4%; SVC: +2.5 to +3.5%, across the tested wind-speed range), rather than reducing them; this reflects the compensators' own reactive power exchange with the network through the bus 9 feeder, which marginally increases I^2X losses on that branch even as it improves local voltage regulation. This differs from the loss-reduction benefit reported for optimal, network-wide reactive power compensation of offshore wind transmission by Rehman et al. [16], and may be attributed to the localised, single-bus placement of the compensator in this study rather than a network-optimised allocation.

Table 1. RMS voltage deviation, reliability, and mean STATCOM output from full N-R simulation (30% penetration). Sys. 1 = No compensation, Sys. 2 = STATCOM, Sys. 3 = SVC

v (m/s)	Vd_1 (%)	Vd_2 (%)	Vd_3 (%)	Rel_1 (%)	Rel_2 (%)	Rel_3 (%)	Qc_STATCOM (MVAr)
3	2.97	0.8	1.08	100	100	100	19.77
5	2.97	0.8	1.08	100	100	100	19.77
7	2.96	0.79	1.07	100	100	100	19.77
9	2.92	0.76	1.04	100	100	100	19.76
12	2.81	0.64	1.16	100	100	100	19.72
15	2.79	0.61	1.01	100	100	100	19.72
18	2.79	0.61	1.02	100	100	100	19.72

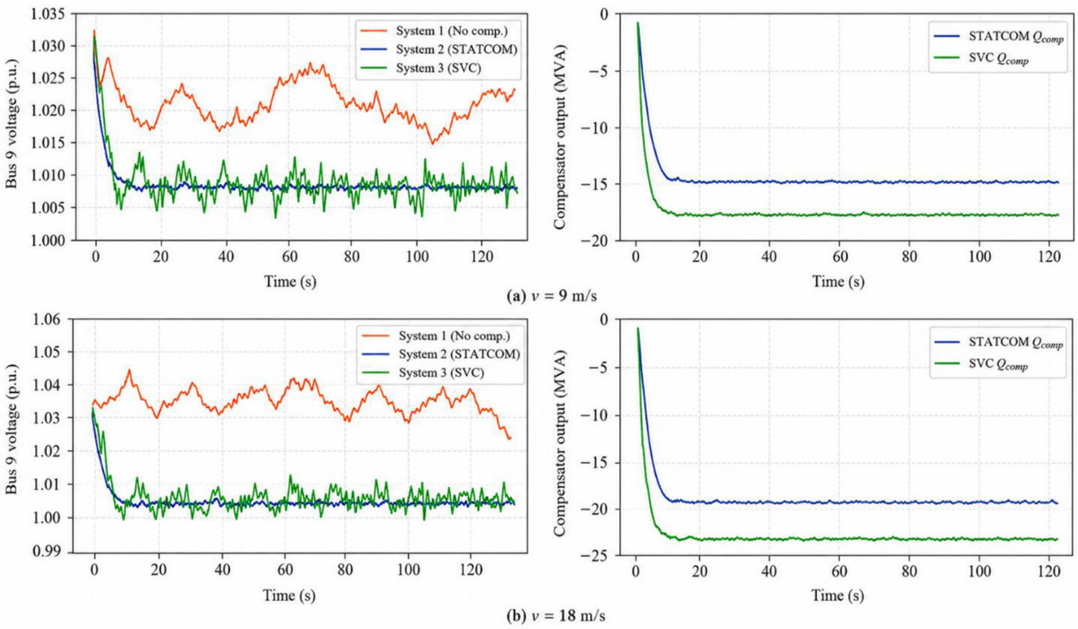

Figure 5. Dynamic bus 9 V (upper) and compensator output (lower) for STATCOM vs. SVC at 9 m/s and 18 m/s. First 120 s shown for clarity

Reactive losses decrease monotonically with wind speed, from a maximum of approximately 64.9 MVAr at cut-in (v = 3 m/s) to a minimum of approximately 49.7 MVAr at and above rated wind speed (v ≥ 15 m/s), reflecting reduced net reactive current draw as the DFIG's active power injection increasingly offsets the local load at Bus 9 as wind speed rises toward rated.

Table 2 shows a clear change in trend around the rated wind speed (12 m/s). Reactive power losses decrease gradually between 3 and 9 m/s, followed by a more pronounced reduction between 9 and 12 m/s, after which they remain nearly constant. This behaviour coincides with the transition of the DFIG from the cubic power region to rated-power operation, resulting in only minor changes in network reactive power flow at higher wind speeds. The same break is visible, though smaller in magnitude, in the VSI columns, which step down from 0.971/0.951/0.953 to 0.970/0.949/0.952 at the same v = 12 m/s point.

Sensitivity analysis: Wind penetration

Figure 7 presents the sensitivity of voltage deviation (Figure 7a) and system reliability (Figure 7b) to wind penetration level at v = 12 m/s. As penetration increases from 10% to 50%, the uncompensated system shows a monotonic decrease in voltage deviation (2.93% to 2.64%). This trend is associated with the increased active power injection from the wind farm, which reduces the effective loading of Bus 9, while turbulence-induced fluctuations scale with penetration. STATCOM performance also improves with increasing penetration, reducing the RMS voltage deviation from 0.76% to 0.48%, owing to its continuous dynamic

Table 2. VSI and system-wide reactive losses (20-branch sum, MVAr) from full N-R simulation

v (m/s)	VSI Sys.1	VSI Sys.2	VSI Sys.3	Q-loss Sys.1 (MVAr)	Q-loss Sys.2 (MVAr)	Q-loss Sys.3 (MVAr)
3	0.971	0.951	0.953	64.89	66.78	66.51
5	0.971	0.951	0.953	64.69	66.57	66.31
7	0.971	0.951	0.953	63.26	65.34	65.03
9	0.971	0.951	0.953	59.23	61.82	61.18
12	0.97	0.949	0.952	51.07	53.18	52.67
15	0.97	0.949	0.952	49.65	51.79	51.37
18	0.97	0.949	0.952	49.65	51.78	51.34

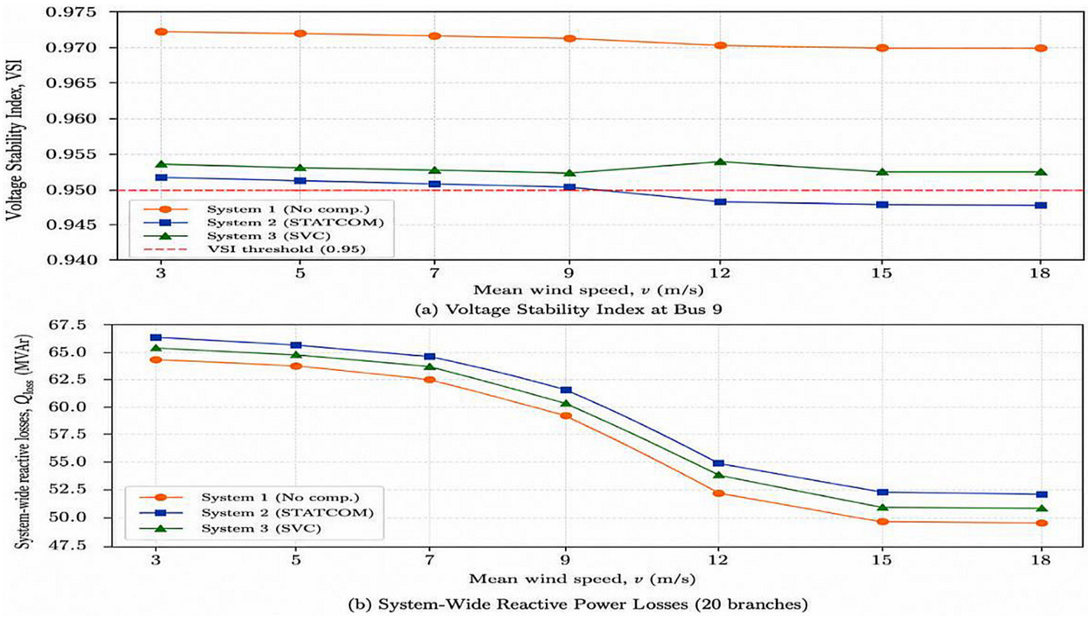

Figure 6. Voltage stability index (a) and system-wide reactive losses over all 20 branches (b) for three compensation strategies

reactive power regulation under higher wind-power injection. SVC performance is non-monotonic, peaking at 30% penetration (1.16%) due to the interaction between its proportional gain and the changing network sensitivity. Both STATCOM and SVC maintain 100% reliability (fraction of time V9 remains within [0.95, 1.05] p.u.) across the entire tested penetration range (10–50%); no reliability degradation was observed for either compensator at any tested penetration level in this benchmark network. Therefore, the comparison between STATCOM and SVC in this study is primarily based on voltage-regulation quality rather than reliability, since both compensators satisfy the adopted reliability criterion under all investigated operating conditions.

Table 3 shows that the two compensators respond to increasing penetration in opposite ways.

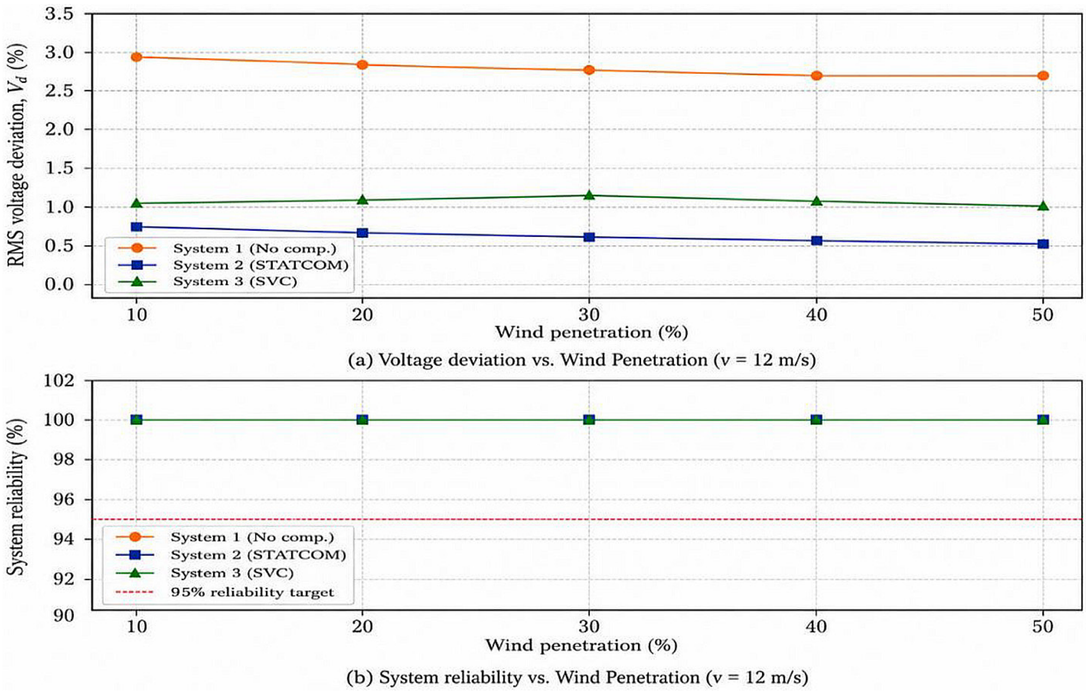

Figure 7. Sensitivity analysis: voltage deviation (a) and reliability (b) for wind penetration (10–50%) at v = 12 m/s. Full N-R IEEE 14-bus simulatio

Table 3. Sensitivity analysis KPIs (v = 12 m/s). Systems 1 = No comp., 2 = STATCOM, 3 = SVC.

Pen. (%)	Vd Sys.1 (%)	Vd Sys.2 (%)	Vd Sys.3 (%)	Rel Sys.1 (%)	Rel Sys.2 (%)	Rel Sys.3 (%)
10	2.93	0.76	1.04	100	100	100
20	2.88	0.71	1.12	100	100	100
30	2.81	0.64	1.16	100	100	100
40	2.74	0.56	1.08	100	100	100
50	2.64	0.48	1.01	100	100	100

Vd_2 (STATCOM) improves monotonically and proportionally more than Vd_1: it falls from 0.76% to 0.48%, a 37% relative reduction, versus only a 10% relative reduction in the uncompensated Vd_1 (2.93% to 2.64%) over the same range. Vd_3 (SVC), in contrast, is non-monotonic. The highest RMS voltage deviation for the SVC occurs at the 30% penetration level, which corresponds to the main operating condition adopted throughout this study.

Voltage distribution at bus 9

Figure 8 shows the boxplots of bus 9 V distribution (% of nominal) for all three configurations across the seven wind-speed operating points. At 30% penetration, all three systems remain above the lower limit (>95%) at every wind speed. The clearest differences appear in the interquartile range (IQR) and whisker length: System 1 (orange, no compensation) shows the widest IQR and longest whiskers, reflecting its full exposure to turbulence-driven voltage variability. System 2 (blue, STATCOM) has the narrowest IQR at every wind speed, consistent with superior turbulence rejection. System 3 (green, SVC) shows an intermediate IQR width, with longer upper whiskers at high wind speeds, consistent with occasional larger transient excursions in the SVC's proportional response under rapid wind-speed fluctuations.

All-bus voltage profile

The full N-R simulation framework captures voltage changes at all buses at once, unlike single-bus equivalent approaches. Figure 9 shows the all-bus voltage profile at v = 12 m/s under 30% penetration for the three configurations. Buses 1, 6, 7, 8, and 12 exceed the 105% upper limit because of the PV bus voltage settings in the IEEE 14-bus base case. In practice, AVR action would correct this, but the published set points are kept here to stay consistent with the benchmark. STATCOM compensation at bus 9 also raises voltages at the adjacent load buses (9, 10, 11, 14) by 0.9–2.2 percentage points. This shows that compensation at one bus affects voltage beyond its own connection point, something single-bus models cannot capture [4]. SVC gives similar but smaller improvements at the same buses (0.7–1.7 percentage points), consistent with its lower and more variable reactive output.

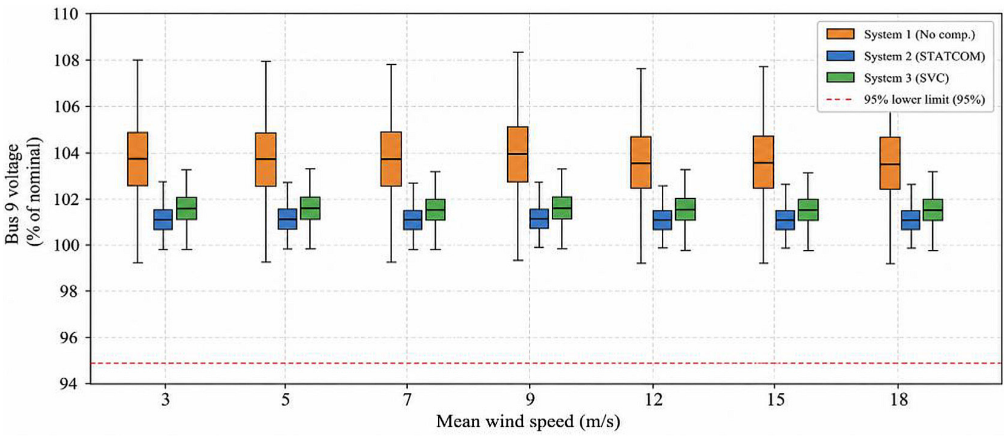

Figure 8. Bus 9 voltage distribution (% nominal) for Systems 1 (No comp.), 2 (STATCOM), 3 (SVC). Full N-R IEEE 14-bus simulation

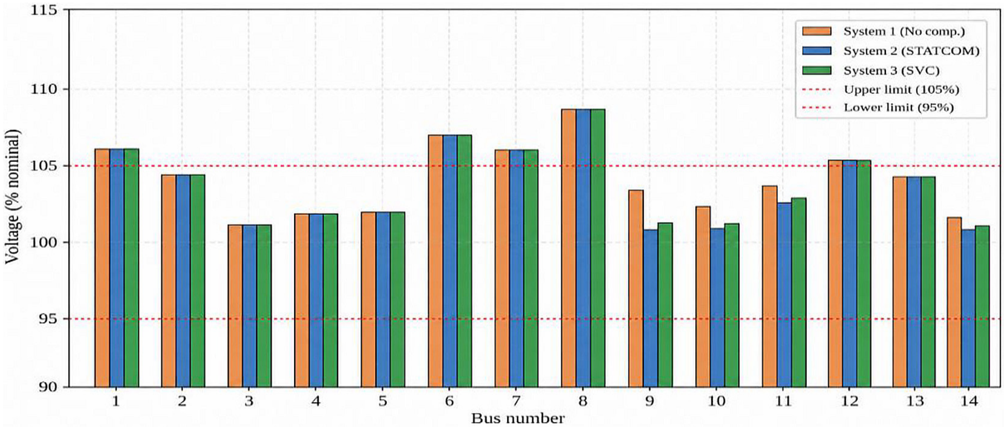

Figure 9. All-bus voltage profile (% nominal) for three compensation strategies at v = 12 m/s, 30% penetration. Full IEEE 14-bus N-R power flow

Monte Carlo statistical validation

To assess the statistical robustness of the proposed approach across multiple random wind-turbulence realisations, the primary wind-speed study (Table 1) was repeated with N = 15 independent AR(1) realisations per operating point (105 simulations per compensation type, 315 in total), using the validated simulation code with an additional independent random seed per replication. Table 4 reports the mean RMS voltage deviation and 95% confidence interval (CI) for each system at each wind speed, together with a two-sided Wilcoxon signed-rank test comparing the paired STATCOM and SVC voltage-deviation samples at each wind speed (the non-parametric Wilcoxon test was used, rather than a paired t-test, because the underlying per-seed differences are not guaranteed to be normally distributed) (Figure 10).

The Monte Carlo results consistently confirm the superior voltage-regulation performance of the STATCOM over the SVC at every investigated operating point ($p < 0.001$, Wilcoxon signed-rank, N = 15), with STATCOM outperforming SVC in all 15 paired replications at every operating point. Reliability remained at 100% for all three systems across all 315 Monte Carlo runs, consistent with the single-realisation results in Section “Voltage deviation and system reliability”. The 95% confidence intervals on the RMS voltage deviation are narrow relative to the STATCOM-SVC performance gap at every wind speed, confirming that the comparison reported in Table 1 is not an artefact of the particular AR(1) realisation used there. This statistical evaluation applies to the primary wind-speed study; the penetration sensitivity study (Table 3) was not repeated with multiple realisations and remains a single-realisation result.

Generalization to a larger network (IEEE 30-Bus)

To examine whether the STATCOM-over-SVC finding generalises beyond a single test system, the same comparison was repeated on the standard IEEE 30-bus benchmark network (bus and branch data taken directly from the official MATPOWER case30.m file), independently of the IEEE 14-bus code used for Tables 1–3. Unlike the IEEE 14-bus model in this study, the standard bus shunts at bus 5 (0.19 p.u.) and bus 24 (0.04 p.u.) are included here, following the published case30 data without modification. The wind farm was connected at bus 30, a radial, electrically remote load bus with no local generation or reactive support, analogous in role to bus 9 in the IEEE 14-bus network: bus 30 connects only to buses 27 and 29 (branches 27–30 and 29–30), confirming its leaf-node, single-feed topology. The same STATCOM and SVC controllers (Equations 7–8) and the same AR(1) wind model (Equation 11) were applied, with wind capacity again scaled as Pr = penetration × sbase (30 MW at 30% penetration). Table 5 reports the resulting KPIs across the same seven wind speeds used in Table 1, using a single AR(1) realisation per point, consistent with the original Table 1 methodology. The results show both similarities to and differences from the IEEE 14-bus network. Vd_1 (no compensation) falls sharply between v = 9 and v = 12 m/s, from 3.722% to 2.499%, a 33% drop in a single step, before flattening out at v = 15–18 m/s (2.297% at both points). This

Table 4. Monte Carlo RMS voltage deviation (mean ± 95% CI, N = 15 independent AR(1) realisations per operating point) and Wilcoxon signed-rank test (STATCOM and SVC, paired by seed) at 30% wind penetration

v (m/s)	Vd Sys.1 (%)	Vd Sys.2 STATCOM (%)	Vd Sys.3 SVC (%)	Wilcoxon p
3	2.971 ± 0.000	0.802 ± 0.000	1.086 ± 0.006	p < 0.001
5	2.970 ± 0.000	0.801 ± 0.000	1.081 ± 0.000	p < 0.001
7	2.960 ± 0.000	0.790 ± 0.001	1.071 ± 0.000	p < 0.001
9	2.929 ± 0.003	0.757 ± 0.003	1.055 ± 0.015	p < 0.001
12	2.815 ± 0.004	0.641 ± 0.003	1.087 ± 0.033	p < 0.001
15	2.789 ± 0.000	0.614 ± 0.000	1.057 ± 0.027	p < 0.001
18	2.789 ± 0.000	0.614 ± 0.000	1.090 ± 0.033	p < 0.001

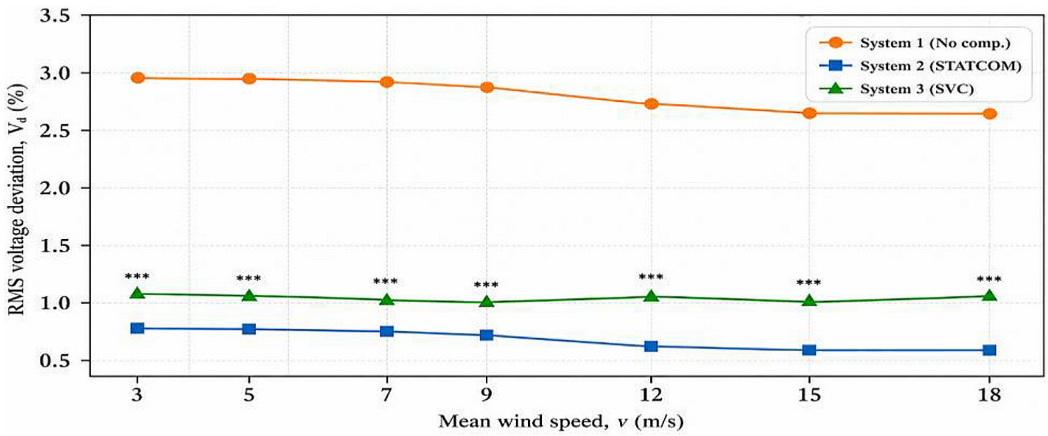

Figure 10. Monte Carlo RMS voltage deviation vs. wind speed (mean ± 95% CI, N = 15 realisations). Asterisks mark $p < 0.001$ (Wilcoxon signed-rank test, STATCOM vs. SVC)

mirrors the rated-speed elbow seen in Table 2, but the effect is more pronounced on this network.Vd_3 (SVC) is markedly non-monotonic and, unlike on the IEEE 14-bus network, reaches its overall maximum away from rated speed: it peaks at v = 15 m/s (1.418%), higher than its value at v = 9 m/s (1.174%) or v = 12 m/s (0.970%), suggesting that the dynamic response of the SVC is influenced by the different impedance characteristics of the IEEE 30-bus network. Unlike the IEEE 14-bus case, the reactive-loss trend differs on the IEEE 30-bus network: rather than decreasing at rated speed, losses rise from about 8.75-9.00 MVAr (v = 3–9 m/s) to 11.40–12.85 MVAr (v = 12–18 m/s), and on this network the STATCOM consistently reduces losses relative to the uncompensated case (e.g. 11.43 vs. 11.94 MVAr at v = 12 m/s, a 4.3% reduction) rather than increasing them as it does on the IEEE 14-bus network (Figure 11).

Table 5. STATCOM and SVC comparison on the IEEE 30-bus network (Bus 30, 30% wind penetration). Vd = RMS voltage deviation, Rel = reliability, Qloss = system-wide reactive loss (41 branches)

v (m/s)	Vd Sys.1 (%)	Vd Sys.2 STATCOM (%)	Vd Sys.3 SVC (%)	Rel (all, %)	Qloss Sys.1 (MVAr)	Qloss Sys.2 (MVAr)	Qloss Sys.3 (MVAr)
3	4.725	0.266	0.896	100	9.00	8.95	8.96
5	4.687	0.263	0.890	100	8.96	8.90	8.91
7	4.421	0.263	1.090	100	8.75	8.65	8.61
9	3.722	0.258	1.174	100	8.79	8.46	8.49
12	2.499	0.211	0.970	100	11.94	11.43	11.40
15	2.297	0.166	1.418	100	12.85	12.32	12.55
18	2.297	0.159	1.017	100	12.85	12.32	12.41

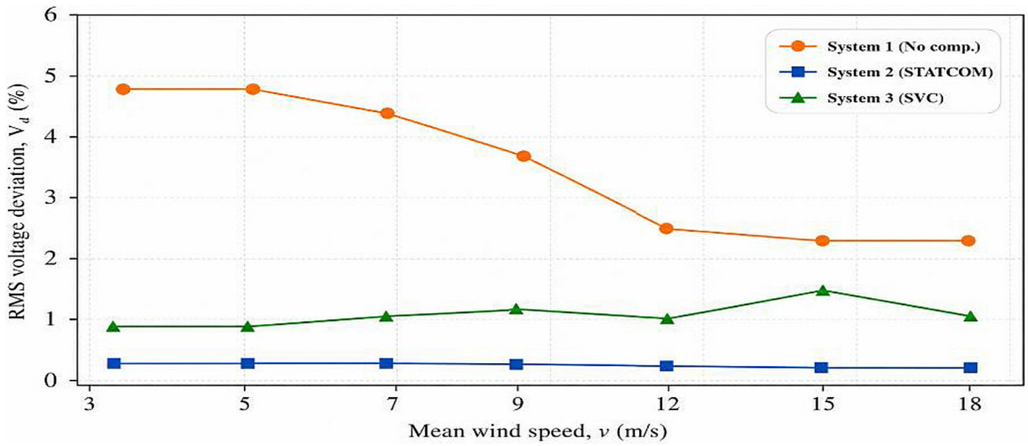

Figure 11. RMS voltage deviation at bus 30 and wind speed, IEEE 30-bus network, 30% penetration

The STATCOM-over-SVC advantage observed on the IEEE 14-bus network reproduces clearly on this independent, larger network: STATCOM reduces RMS voltage deviation to 0.16–0.27% versus 0.89-1.42% for SVC across all seven wind speeds – a larger relative advantage than on the IEEE 14-bus network, consistent with Bus 30's weaker local voltage support. Reliability again stays at 100% for both compensators throughout, consistent with the IEEE 14-bus result. Reactive losses on this network are close to unchanged by compensation (within ±1 MVAr of the uncompensated case at most wind speeds), rather than showing the small increase observed on the IEEE 14-bus network, illustrating that the loss impact of local reactive compensation is network-dependent. This generalisation check used a single AR(1) realisation per operating point (matching the original Table 1 methodology) rather than the N = 15 Monte Carlo replications; a full Monte Carlo validation on the IEEE 30-bus network remains future work, and the present generalisation check therefore complements, rather than replaces, the Monte Carlo validation.

CONCLUSIONS

This paper presented a time-domain simulation study comparing STATCOM and SVC for reactive power compensation and voltage stability in a wind-integrated power system, using a full Newton-Raphson power-flow solution at each time step on the IEEE 14-bus benchmark network. Across seven wind speeds and five penetration levels, the PI-controlled STATCOM consistently achieved a lower RMS voltage deviation at Bus 9 than the SVC, while both compensators maintained full system reliability. This voltage-regulation advantage was statistically confirmed through a Monte Carlo analysis of independent wind-turbulence realisations and was reproduced on an independent, larger IEEE 30-bus network, indicating that the finding is not specific to a single random wind sequence or a single benchmark system. Compensation at Bus 9 also improved voltages at electrically adjacent buses, illustrating network-wide interactions that single-bus equivalent models cannot capture, while system-wide reactive losses were only marginally affected by either compensator. Because both technologies satisfied the adopted reliability criterion under all investigated conditions, the STATCOM's advantage over the SVC rests specifically on the quality of its dynamic voltage regulation rather than on reliability. These findings support the application of STATCOM as an effective solution for improving voltage regulation in wind-integrated transmission networks, and provide a reproducible, full-network simulation framework for evaluating reactive power compensation strategies under realistic wind variability.

REFERENCES

1. Mastoi M. S., Zhuang S., Haris M., Hassan M., and Ali A., (2023). Large-scale wind power grid integration challenges and their solution: a detailed review, *Environmental Science and Pollution Research, 30*, 103424–103462, https://doi.org/10.1007/s11356-023-29653-9
2. Tumse S., Bilgili M., Yildirim A., and Şahin B., (2024). Comparative analysis of global onshore and offshore wind energy characteristics and

potentials, *Sustainability, 16*(15), 6614, https://doi.org/10.3390/su16156614

3. Yadav V. V. et al., (2022). Technical advances and stability analysis in wind-penetrated power generation systems—A review, *Frontiers in Energy Research, 10*, 1091512, https://doi.org/10.3389/fenrg.2022.1091512
4. Ali J. S., Qiblawey Y., Alassi A., Massoud A. M., Muyeen S. M., and Abu-Rub H., (2025). Power system stability with high penetration of renewable energy sources: Challenges, assessment, and mitigation strategies, *IEEE Access, 13*, 39912–39934, https://doi.org/10.1109/ACCESS.2025.3546491
5. Sharma S., Gupta S., Zuhaib M., Bhuria V., Malik H., Almutairi A., Afthanorhan A., and Hossaini M. A., (2024). A comprehensive review on STATCOM: Paradigm of modeling, control, stability, optimal location, integration, application, and installation, *IEEE Access, 12*, 2701–2729, https://doi.org/10.1109/ACCESS.2023.3345216
6. Yang N.-C. and Chang Z.-H., (2023). Optimal capacity and location for STATCOM with seasonal wind power prediction using C-Vine copula, *Mathematics, 11*(13), 2815, https://doi.org/10.3390/math11132815
7. Al-Majali B. H. and Zobaa A. F., (2024). A novel optimal allocation of STATCOM to enhance voltage stability in power networks, *Ain Shams Engineering Journal, 15*(5), 102658, https://doi.org/10.1016/j.asej.2024.102658
8. Adetokun B. B. and Muriithi C. M., (2021). Application and control of flexible alternating current transmission system devices for voltage stability enhancement of renewable-integrated power grid: A comprehensive review, *Heliyon, 7*(3), e06461, https://doi.org/10.1016/j.heliyon.2021.e06461
9. Alajrash B. H., Salem M., Swadi M., Senjyu T., Kamarol M., and Motahhir S., (2024). A comprehensive review of FACTS devices in modern power systems: Addressing power quality, optimal placement, and stability with renewable energy penetration, *Energy Reports, 11*, 5350–5371, https://doi.org/10.1016/j.egyr.2024.05.011
10. Gao et al., (2025). A review of dynamic voltage support for power grids with large-scale penetration of renewable generation, *Frontiers in Energy Research, 13*, 1606725, https://doi.org/10.3389/fenrg.2025.1606725
11. Khan M., Wu W., and Li L., (2024). Grid-forming control for inverter-based resources in power systems: A review on its operation, system stability, and prospective, *IET Renewable Power Generation, 18*, 887–907, https://doi.org/10.1049/rpg2.12991
12. Mahmoud M. M. et al., (2023). Integration of wind systems with SVC and STATCOM during various events to achieve FRT capability and voltage stability: Towards the reliability of modern power systems, *International Journal of Energy Research, 2023*, 8738460, https://doi.org/10.1155/2023/8738460
13. Sadiq R. et al., (2021). A review of STATCOM control for stability enhancement of power systems with wind/PV penetration: Existing research and future scope, *International Transactions on Electrical Energy Systems, 2021*, 5560916, https://doi.org/10.1002/2050-7038.13079
14. Chirani et al., (2026). Stability analysis of a grid-connected DFIG wind farm using static VAR compensator, *Journal of Electrical and Computer Engineering,* 3210857, https://doi.org/10.1155/jece/3210857
15. Tariq H., Czapp S., Tariq S., Cheema K. M., Hussain A., Milyani A. H., Alghamdi S., and Elbarbary Z. M. S., (2022). Comparative analysis of reactive power compensation devices in a real electric substation, *Energies, 15*(12), 4453, https://doi.org/10.3390/en15124453
16. Rehman A., Koondhar M. A., Ali Z., Jamali M., and El-Sehiemy R. A., (2023). Critical issues of optimal reactive power compensation based on an HVAC transmission system for an offshore wind farm, *Sustainability, 15*(19), 14175, https://doi.org/10.3390/su151914175
17. Sakipour R. and Abdi H., (2022). Voltage stability improvement of wind farms by self-correcting static volt-ampere reactive compensator and energy storage, *International Journal of Electrical Power & Energy Systems, 141*, 108082, https://doi.org/10.1016/j.ijepes.2022.108082
18. Muisyo I. N., Muriithi C. M., and Kamau S. I., (2022). Enhancing low voltage ride through capability of grid connected DFIG based WECS using WCA-PSO tuned STATCOM controller, *Heliyon, 8*(8), e09999, https://doi.org/10.1016/j.heliyon.2022.e09999
19. Borah B., Rajak M. K., Banerjee A., Pudur R., and Deepa S. N., (2026). Enhanced grid stability of DFIG-based wind systems through intelligent reactive power coordination using machine learning-based control, *Scientific Reports, 16*, 17000, https://doi.org/10.1038/s41598-026-47806-x
20. Hiwarkar C. S., Halmare A. M., Belsare A. A., Mohriya N. B., and Milmile R., (2022). Load flow analysis on IEEE 14 bus system, *International Journal for Research in Applied Science & Engineering Technology, 10*(4), 2178–2184, https://doi.org/10.22214/ijraset.2022.41590
21. Hoke A., Gevorgian V., Shah S., Koralewicz P., Kenyon R. W., and Kroposki B., (2021). Island power systems with high levels of inverter-based resources: Stability and reliability challenges, *IEEE Electrification Magazine, 9*(1), 74–91, https://doi.

org/10.1109/MELE.2020.3047169

22. Ranjan M. and Shankar R., (2022). A literature survey on load frequency control considering renewable energy integration in power system: Recent trends and future prospects, *Journal of Energy Storage, 45*, 103717, https://doi.org/10.1016/j.est.2021.103717
23. Al-Zubaydi N. A. H. and Kadhim K. H., (2023). Performance of intelligent wind turbine pitch control through PI, PID, and LQR and hybrid of PI and LQR controllers, *International Journal of Intelligent Systems and Applications in Engineering, 11*(10s), 923–941.
24. Hatziargyriou N., Milanović J., Rahmann C., Ajjarapu V., Cañizares C., Erlich I., Hill D., Hiskens I., Kamwa I., Pal B., Pourbeik P., Sanchez-Gasca J., Stanković A., Van Cutsem T., Vittal V., and Vournas C., (2021). Definition and classification of power system stability – Revisited & extended, *IEEE Transactions on Power Systems, 36*(4), 3271–3281, https://doi.org/10.1109/TPWRS.2020.3041774
25. Micev M., Ćalasan M., and Radulović M., (2023). Optimal tuning of the novel voltage regulation controller considering the real model of the automatic voltage regulation system, *Heliyon, 9*(8), e18707, https://doi.org/10.1016/j.heliyon.2023.e18707
26. Teimourian H., Abubakar M., Yildiz M., and Teimourian A., (2022). A comparative study on wind energy assessment distribution models: A case study on Weibull distribution, *Energies, 15*(15), 5684, https://doi.org/10.3390/en15155684
27. Desalegn B., Gebeyehu D., and Tamrat B., (2022). Evaluating the performances of PI controller (2DOF) under linear and nonlinear operations of DFIG-based WECS: A simulation study, *Heliyon, 8*(11), e11912, https://doi.org/10.1016/j.heliyon.2022.e11912
28. Wu Y.-K., Gau D.-Y., and Tung T.-D., (2023). Overview of various voltage control technologies for wind turbines and AC/DC connection systems, *Energies, 16*(10), 4128, https://doi.org/10.3390/en16104128
29. Shawqran A. M., El-Marhomy A., Attia M. A., Abdelaziz A. Y., and Alhelou H. H., (2021). Enhancement of wind energy conversion system performance using adaptive fractional order PI blade angle controller, *Heliyon, 7*(10), e08239, https://doi.org/10.1016/j.heliyon.2021.e08239